IEEE Access
Multidisciplinary | Rapid Review | Open Access Journal

Received 27 April 2023, accepted 21 May 2023, date of publication 29 May 2023, date of current version 6 June 2023.

*Digital Object Identifier 10.1109/ACCESS.2023.3280911*

RESEARCH ARTICLE

# Influence of Different Control Parameters on the Flux Density and Loss of Stator Core in the Switched Reluctance Motor

**HAN JICHAO, WANG JIAOYU, GE BAOJUN, QI HAIMING, AND BIAN XIZHAO**
School of Electrical and Electronic Engineering, Harbin University of Science and Technology, Harbin 150080, China

Corresponding author: Han Jichao (hanjichao163@163.com)

This work was supported in part by the National Natural Science Foundation of China under Grant 52177037, in part by the Natural Science Foundation of Heilongjiang Province of China under Grant YQ2021E037, and in part by the Research Foundation of State Key Laboratory of Hydro-Power Equipment under Grant SKLHE-ORF-202001.

**ABSTRACT** Switched reluctance motor has the advantages of the high efficiency, low cost, strong fault tolerance, and high reliability. A 5.5 kW, 12/8 pole switched reluctance motor is designed. The novel transient electromagnetic field-control circuit coupled calculation method of switched reluctance motor is proposed. The influence of different PWM switching angles, chopping current thresholds, and hysteresis current widths on flux density and loss of stator core in the switched reluctance motor is studied in detailed by this novel method. Controller harmonics are considered during this calculation. The change of the flux density and loss of stator core in the switched reluctance motor is compared and analyzed under the different controller parameters. The reliability of the calculation method and accuracy of the calculation results are verified by experimental values.

**INDEX TERMS** Switched reluctance motor, calculation method, different control parameters, flux density, loss, stator core.

## I. INTRODUCTION

Switched reluctance motor (SRM) has many advantages, such as the reliable structure, many controllable parameters, and high efficiency in a wide speed range. There is no winding in the rotor. They are highly competitive in the field of electrical drives for the high reliability requirement. The flux density is non-sinusoidal in the stator core of switched reluctance motor during the long-time operation. High-power density switched reluctance motor has the high flux density, stator core loss, and temperature rise, which could affect the safe operation and service life of the switched reluctance motor. Furthermore, the flux density and loss of stator core in the high-power density switched reluctance motor are closely related to the SRM control parameters. It is necessary to study the influence of different controller parameters on the flux density and loss of stator core in the switched reluctance motor.

Extensive studies are performed on the multi-physics field in the switched reluctance motor. The flux density and losses of the switched reluctance motor are studied by some scholars. Core loss analysis of the planar switched reluctance motor is calculated based on the 3-D time-stepping finite element methods. However, the influence of the controller harmonics on the loss of planar switched reluctance motor is not considered in the study [1]. An equivalent circuit-based determination of iron loss is presented. The existence of an eddy current is additionally highlighted. The influence of current chopping parameters on the stator core loss is ignored in the process of calculation [2]. The influence of the stress induced by shrink fitting on the quasi-static hysteresis losses in a switched reluctance motor made of initially isotropic nonoriented iron-silicon sheets is studied. The design and manufacture of SRM are important. The SRM needs to be designed and manufactured reasonably in this paper [3].

The associate editor coordinating the review of this manuscript and approving it for publication was Xiaodong Liang.

A combined design of experiments and differential evolution approach is proposed to identify the designs that produce the target torque with minimum loss and mass. However, the influence of control parameters on the core loss is not considered [4]. A comprehensive investigation method for loss calculation and temperature rise prediction in high-speed and high-power switched reluctance machines is proposed. Accurate calculation of loss is the basis of the accurate calculation of temperature distribution in the SRM [5]. The electromagnetic design aspects of two candidate SRM topologies in a six-phase context for a pure electric or hybrid electric vehicle type application are investigated. Reasonable design is the key of the long-term stable operation of SRM [6]. To evaluate the effects of different rotor topologies, the electromagnetic performances of two modular switched reluctance motors and a conventional SRM with the same basic dimensions are analyzed and compared. Electromagnetic performance, losses, and flux density are important evaluation indicators of SRM [7]. A novel multi-tooth hybrid-excited switched reluctance motor is proposed. Finite element analysis is adopted to obtain the static characteristics of the motor in terms of magnetic flux density, flux linkage, inductance, and torque profiles. It shows that the finite element method can accurately calculate the electromagnetic field, flux density, loss, and torque of SRM [8]. An approach to eliminate the mutual flux effect on the rotor position estimation of switched reluctance motor drives without a priori knowledge of mutual flux is proposed. How to reduce the mutual flux effect and loss is the key to SRM design [9]. The iron loss of the doubled-sided linear switched reluctance motor is studied. However, influence of control parameters on the iron core loss is ignored in this study [10]. The magnetic equivalent circuit model of two-phase SRM is proposed. The electromagnetics torque, flux density, inductance, flux linkage, and peak torque are evaluated and the performance of SRM is studied. The accurate calculation of flux density is the foundation of SRM design [11]. The double stator switched reluctance machine is proposed. The efficiency, torque ripple, flux density, vibration and noise, and fault tolerance of this switched reluctance machine are researched. The flux density and losses are key design parameters for SRM [12]. The core loss reduction by the application of a zero-voltage loop period is assessed with FE modeling and simulation of 12/8 SRM. The core loss reduction mechanism is clarified by the evaluation of the flux density at specific points in the SRM core. However, the influence of the hysteresis current width on the core loss of SRM is neglected [13]. A novel 12/14 SRM is studied using FEA. The main characteristics of this SRM including mean and peak torque, flux density, and torque ripple are compared with those of conventional SRM. However, influence of control parameters on flux density and losses is not considered in this study [14]. Some other experts also studied the multi-physics field of switched reluctance motor [15], [16], [17], [18], [19], but very few focused on the influence of different control parameters on the flux density and loss of the stator core in the switched reluctance motor.

In this paper, the novel transient electromagnetic field-control circuit coupled calculation method of SRM is proposed. A 5.5 kW SRM is studied. The influence of the controller harmonics on the flux density and losses of switched reluctance motor is not considered in the traditional calculation method. Controller harmonics are considered during the calculation in this paper. The speed closed loop and current closed loop are considered in the transient electromagnetic field-control circuit coupled calculation method to perform system level calculation. The flux density and losses of switched reluctance motor are calculated by taking into account the controller harmonics and the actual operation of the control system. The loss of stator core in the SRM can be accurately obtained. Based on the transient electromagnetic field-control circuit coupled calculation method of switched reluctance motor, the influence of different PWM switching angles, chopping current thresholds, and hysteresis current widths on flux density and loss of stator core in the switched reluctance motor is studied in detailed in this paper. The change of the flux density and loss of stator core in the SRM is compared and analyzed under the different controller parameters. The accuracy of the calculation results and the reliability of the calculation method are verified by experimental values. It provides a reference for the optimization of design and controller parameter of SRM.

## II. NOVEL TRANSIENT ELECTROMAGNETIC FIELD-CONTROL CIRCUIT COUPLED CALCULATION METHOD OF SRM

In this paper, 5.5kW SRM is studied. Fig. 1 shows the two-dimensional finite element model of SRM. The basic parameters of this 5.5kW SRM are shown in Table 1.

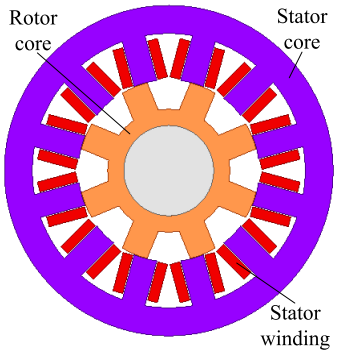


**FIGURE 1.** Two-dimensional finite element model of SRM.

The mathematical equations of the two-dimensional electromagnetic field of the SRM are given as follows:

$$\begin{cases} \Omega : \dfrac{\partial}{\partial x}\left(\dfrac{1}{\mu}\dfrac{\partial A_z}{\partial x}\right) + \dfrac{\partial}{\partial y}\left(\dfrac{1}{\mu}\dfrac{\partial A_z}{\partial y}\right) = -J_z + \sigma\dfrac{\partial A_z}{\partial t} \\ A_z|_\Gamma = 0 \end{cases} \quad (1)$$

where $A_z$ is vector magnetic potential. $J_z$ is the source current density (in A/m$^2$), $\mu$ is the permeability (in H/m), $\sigma$ is the conductivity (in S/m).

**TABLE 1. Basic parameters of this 5.5kW SRM.**

| Parameters | Value |
|---|---|
| Stator outer diameter(mm) | 210.7 |
| Stator inner diameter(mm) | 116 |
| Rotor outer diameter(mm) | 115.2 |
| Rotor inner diameter(mm) | 57.6 |
| Stator arc(°) | 15 |
| Rotor arc(°) | 16 |
| Turns per pole | 130 |
| Air gap(mm) | 0.4 |
| Stator core length(mm) | 130.8 |
| Stator yoke thickness(mm) | 17.9 |

In this paper, speed and current double-closed-loop drive circuit of SRM includes the speed feedback, current feedback, SRM, rotor position detection device, and drive trigger circuit. Fig. 2 shows the block diagram of the SRM drive circuit. On the premise of ensuring calculation accuracy, 2D FE modeling is used to save the calculation time.

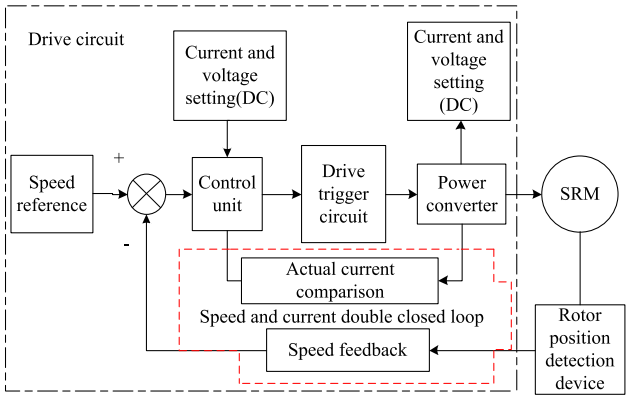


**FIGURE 2. Block diagram of the SRM drive circuit.**

The current chopper control (CCC) and voltage PWM control is adopted in the SRM, which can effectively track the current and reduce current ripple. Current chopper control is used in the start-up process and the start-up current is limited by the SRM drive circuit. Fig. 3 shows the speed and current dual closed-loop drive circuit of SRM. The SRM drive circuit control strategy is implemented by the current chopper control and voltage PWM control. The reference current calculation module consists of blocks GAIN1, REF, KP, KI and LIMIT. The gain block GAIN1 converts the radian values into the angular values. The reference speed is set by block REF, block KP, and block KI. The signal limiter module limits the input signal and sets the upper and lower limit values. The block IA, block IB, and block IC are the feedback currents. The position detection module consists of blocks GAIN2, E, CONST and comparator. The block GAIN2 converts the angular velocity values into the speed values. The block E establishes the relationship between input and output. The block CONST sets the signal source to the constant value. The double closed-loop drive control method of the SRM is adopted in this paper. It includes the current inner loop control and the speed outer loop control.

The influence of the controller harmonics on the loss of SRM is considered during the calculation. The loss of stator core in the switched reluctance motor is accurately determined. Flux density is closely related to loss of stator core. It is necessary to determine accurately the flux density of the stator core in the SRM. In order to calculate accurately the loss of stator core, sample points in the stator core are selected to analyze the flux density of stator core under the different controller parameters. Fig. 4 shows the flux distribution in the SRM. The sample line AB is selected. The sample point A is located at the top of the stator tooth. The sample point B is located in the stator yoke. In order to study the influence of different control parameters on the loss of the stator core of SRM in detail, the stator core is divided into some parts. In Fig. 5, zone SY1, zone SY2, zone SY3, and zone SY4 represent the stator outer yoke, stator inner yoke, stator tooth body, and stator tooth top, respectively. Based on the transient electromagnetic field-control circuit coupled calculation method of switched reluctance motor, the influence of different PWM switching angles, chopping current thresholds, and hysteresis current widths on the flux density and loss of stator core in the SRM is studied in this paper [20], [21], [22], [23], [24].

## III. INFLUENCE OF DIFFERENT CONTROL PARAMETERS ON THE FLUX DENSITY AND LOSS OF THE STATOR CORE IN THE SRM BASED ON NOVEL CALCULATION METHOD

As can be seen from Table 2, the PWM switching angle, the chopping current, and the hysteresis current width is 16°, 45A, and 0.2 A in the SRM under the rated operating condition. Three typical values are selected from the PWM switching angle, chopping current, and hysteresis current width, respectively. The influence of the typical PWM switching angles, chopping current thresholds, and hysteresis current widths on flux density and loss of stator core in the switched reluctance motor is studied in detailed by the novel calculation method. 14°, 15°, and 16° are three typical values of PWM switching angle. When the PWM switching angle is greater than 16°, it will widen the commutation overlap area of SRM. The total current increases in the commutation overlapping area. The torque is generated in each commutation overlapping area of SRM, which leads to significant torque ripple during the operation. When the PWM switching angle is less than 14°, it will lead to a decrease in the efficiency of SRM. 40A, 45A, and 50A are three typical values of chopping current. When the chopping current is greater than 50A, it may cause damage to electronic devices. When the chopping current is less than 40A, it will result in a slower increase in rotor speed during the starting process of the SRM. 0.1A, 0.2A, and 0.3A are three typical values of hysteresis current width. When the hysteresis current width is greater than 0.3A, it will cause current fluctuations. When

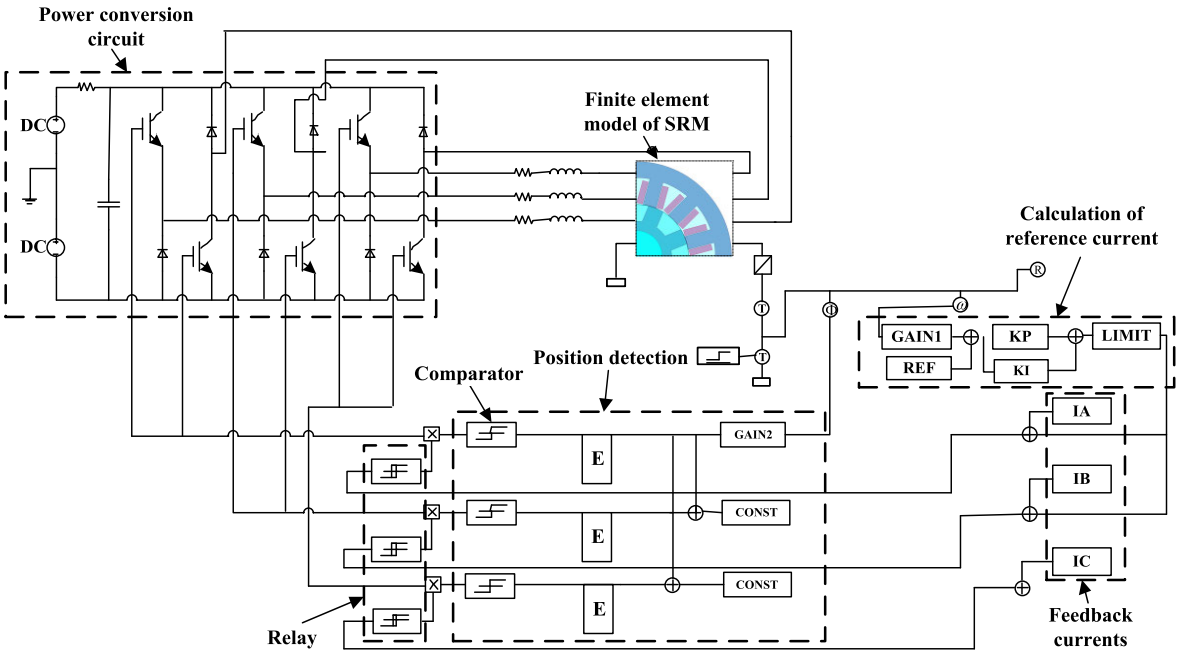


**FIGURE 3.** Speed and current double-closed-loop drive circuit of SRM.

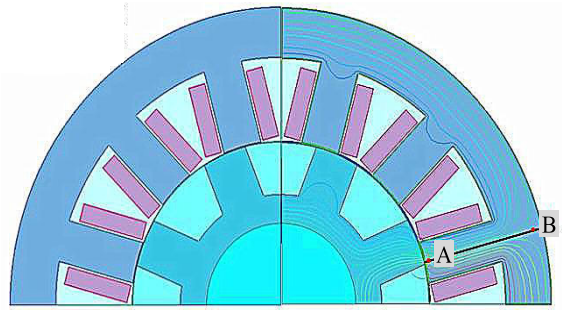


**FIGURE 4.** Flux distribution in the SRM.

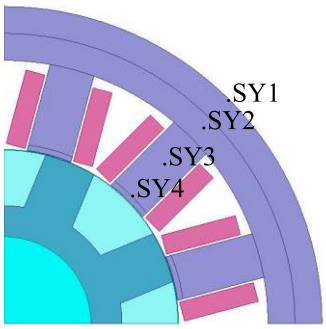


**FIGURE 5.** Location of sample points in the stator core.

the hysteresis current width is less than 0.1A, this will cause a high switching frequency of the switch transistor. It reduces the service life of the switch transistor. The influence of the typical PWM switching angles, chopping currents, and hysteresis current widths on flux density and loss of stator core in the SRM is obtained.

**TABLE 2.** Basic parameters in the control circuit.

| Basic parameters | |
|---|---|
| Inductance (mH) | 0.173934 |
| Resistance (Ω) | 0.788297 |
| PWM switching angle (°) | 16 |
| Chopping current (A) | 45 |
| Hysteresis current width (A) | 0.2 |

### *A. INFLUENCE OF PWM SWITCHING ANGLE ON FLUX DENSITY AND LOSS OF STATOR CORE*

Fig. 6 shows the radial and tangential flux density of the stator core at point A and point B when PWM switching angle is 16°, 15°, and 14°, respectively. In Fig. 6 (a), it can be seen that the radial flux density distribution is related to PWM switching angle at point A and point B. Table 3 gives the average values of the radial and tangential flux density at point A and point B under the different PWM switching angles.

It can be seen from Table 3 that the average value of the radial flux density at point A is the highest under the different PWM switching angles. The average value of the radial flux density decreases with the decrease of the PWM switching angle at point A. The average value of the tangential flux density increases with the decrease of the PWM switching angle at point A. The average value of the radial flux density is almost constant at point B when the PWM switching angles are 15° and 14°, respectively. The average value of

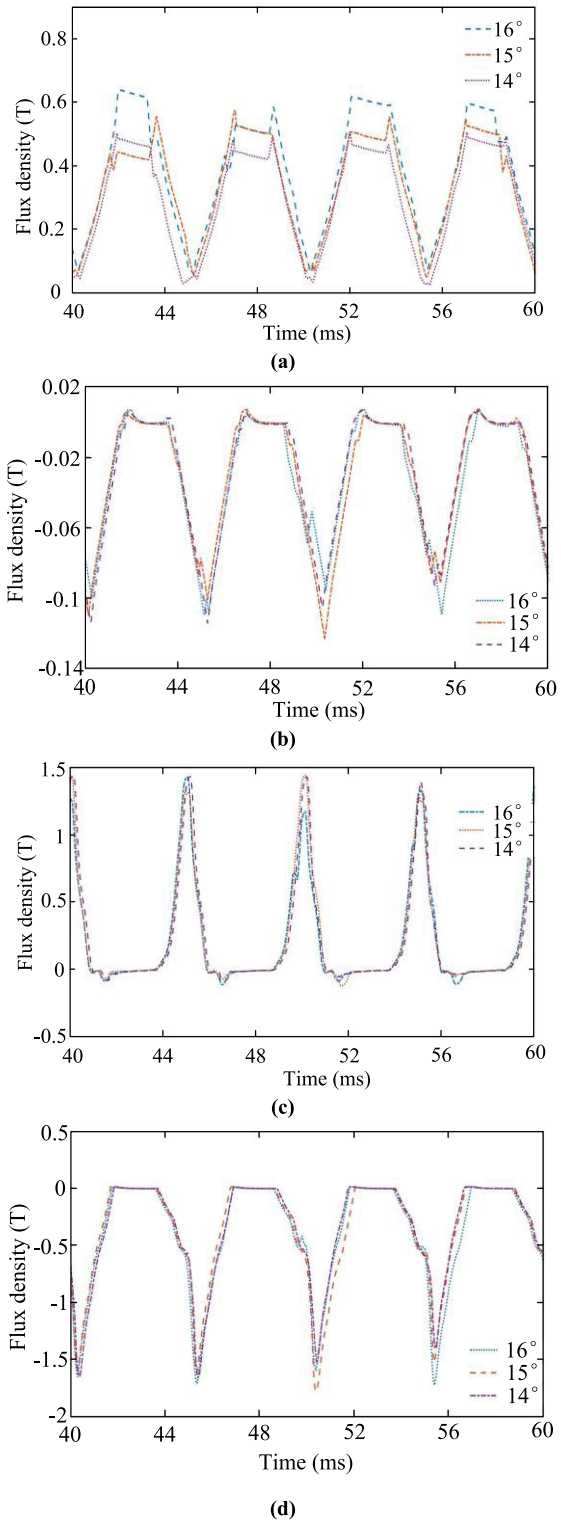


**FIGURE 6.** Radial and tangential flux density of the stator core at point A and point B when PWM switching angle is 16°, 15°, and 14°, respectively. (a) Radial flux density at point A. (b) Tangential flux density at point A. (c) Radial flux density at point B. (d) Tangential flux density at point B.

the tangential flux density increases with the decrease of the PWM switching angle at point B.

**TABLE 3.** Average values of the radial and tangential flux density at point A and point B under the different PWM switching angles.

| Flux density (T) | PWM switching angle (°) | | |
|---|---|---|---|
| | 16° | 15° | 14° |
| Radial flux density at point A | 0.3943 | 0.3490 | 0.3001 |
| Tangential flux density at point A | -0.0316 | -0.0306 | -0.0292 |
| Radial flux density at point B | 0.2139 | 0.2199 | 0.2198 |
| Tangential flux density at point B | -0.3929 | -0.3732 | -0.3517 |

**TABLE 4.** Loss of stator core at different zones under the different PWM switching angles.

| PWM switching angle (°) | Losses of different regions (W) | | | | |
|---|---|---|---|---|---|
| | Stator tooth top | Stator tooth body | Stator inner yoke | Stator outer yoke | Total stator core |
| 16° | 6.75 | 43.51 | 24.55 | 13.71 | 88.52 |
| 15° | 6.32 | 40.03 | 22.98 | 12.40 | 81.73 |
| 14° | 6.07 | 38.34 | 21.87 | 10.19 | 77.11 |

Table 4 shows the loss of stator core at different zones under the different PWM switching angles. It can be seen from Table 4 that the total loss of stator core is 88.52W, 81.73W, and 77.11W when the PWM switching angle is 16°, 15°, and 14° under the rated operating condition. The losses of stator tooth top, stator tooth body, stator inner yoke, and stator outer yoke when PWM switching angle is 15° are 6.4%, 8%, 6.4%, and 9.6% lower than those of stator tooth top, stator tooth body, stator inner yoke, and stator outer yoke when PWM switching angle is 16°. It can be seen that the loss change of the stator outer yoke is obvious. The losses of stator tooth top, stator tooth body, stator inner yoke, and stator outer yoke when PWM switching angle is 14° are 4%, 4.2%, 4.8%, and 9.6% lower than those of stator tooth top, stator tooth body, stator inner yoke, and stator outer yoke when PWM switching angle is 15°. The total loss of stator core when PWM switching angle is 14° are 5.7% lower than that of stator core when PWM switching angle is 15°.

### B. INFLUENCE OF CHOPPING CURRENT THRESHOLD ON FLUX DENSITY AND LOSS OF STATOR CORE

The starting current is limited by the control circuit in the start-up process. The chopping current threshold is the key parameter. If the chopping current is changed, the flux density is affected in the SRM. Fig. 7 shows the radial and tangential flux density of the stator core at point A and point B when the chopping current thresholds are 50A, 45A, and 40A, respectively.

It can be seen from Fig. 7 (a) that the radial flux density is related to the chopping current threshold at point A. When the chopping current threshold is 45 A, the peak value of radial flux density is higher at point A. Table 5 shows the average values of the radial and tangential flux density at point A and point B under the different chopping current thresholds. It can be seen from Table 5 that the difference of the radial flux

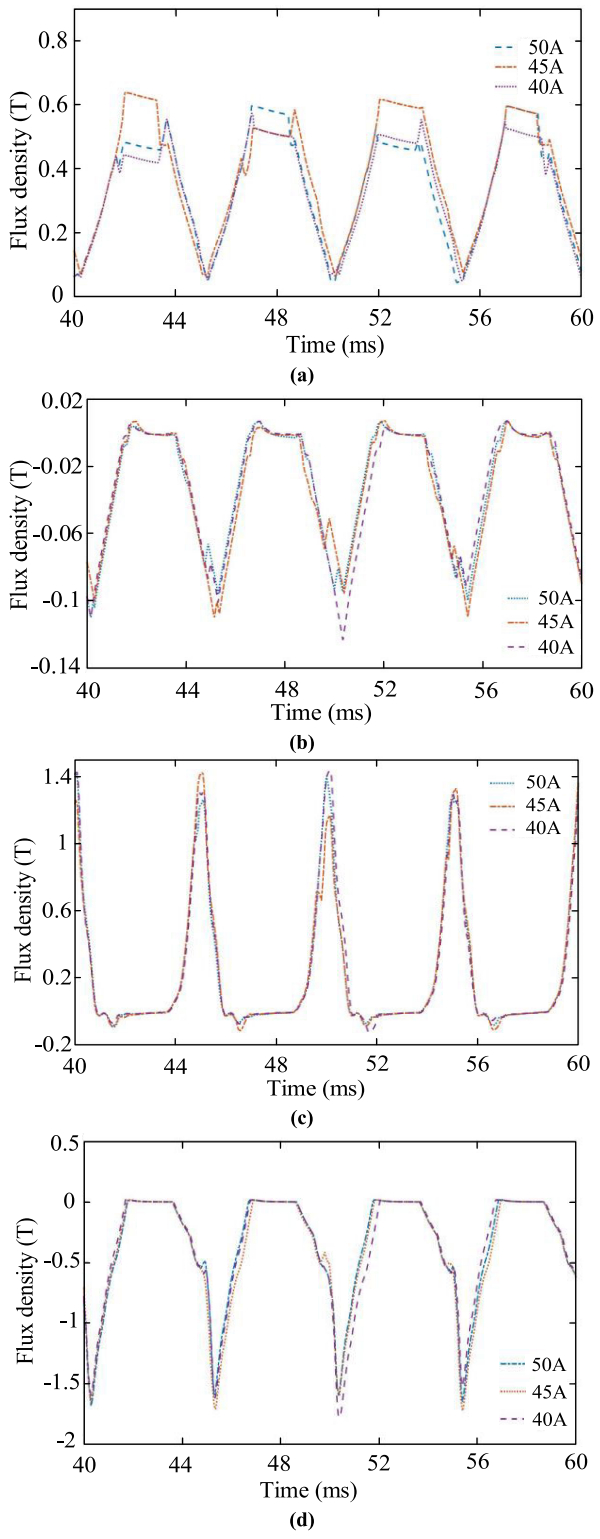


**FIGURE 7.** Radial and tangential flux density of the stator core at point A and point B when the chopping current thresholds are 50A, 45A, and 40A, respectively. (a) Radial flux density at point A. (b) Tangential flux density at point A. (c) Radial flux density at point B. (d) Tangential flux density at point B.

density at point A is obvious under the different chopping current thresholds. Radial flux density and tangential flux density at point A are the largest when the chopping current threshold is 45A.

**TABLE 5.** Average values of the radial and tangential flux density at point A and point B under the different chopping current thresholds.

| Flux density (T) | Chopping current threshold (A) | | |
|---|---|---|---|
| | 50A | 45A | 40A |
| Radial flux density at point A | 0.3508 | 0.3843 | 0.3402 |
| Tangential flux density at point A | -0.0300 | -0.0316 | -0.0306 |
| Radial flux density at point B | 0.2175 | 0.2139 | 0.2199 |
| Tangential flux density at point B | -0.3685 | -0.3929 | -0.3733 |

**TABLE 6.** Loss of stator core at different zones under the different chopping current thresholds.

| Chopping current threshold (A) | Losses of different regions (W) | | | | |
|---|---|---|---|---|---|
| | Stator tooth top | Stator tooth body | Stator inner yoke | Stator outer yoke | Total loss of stator core |
| 50A | 6.72 | 43.27 | 24.41 | 13.61 | 88.01 |
| 45A | 6.75 | 43.51 | 24.55 | 13.71 | 88.52 |
| 40A | 6.65 | 44.19 | 24.33 | 13.60 | 88.77 |

The loss of the stator core is calculated as follows.

$$P_e = k_h f B_m^2 + k_c f^2 B_m^2 + k_e f^{1.5} B_m^{1.5} \tag{2}$$

where $k_h$ is hysteresis coefficient. $k_c$ is classical eddy current coefficient. $k_e$ is excess eddy current coefficient. $B_m$ is amplitude of the flux density. $f$ is frequency.

Table 6 shows the loss of stator core at different zones under the different chopping current thresholds. It can be seen from Table 6 that the influence of the chopping current threshold on the stator core loss is not obvious. As the chopping current threshold decreases, the total loss of stator core increases. The loss of stator tooth body when the chopping current threshold is 40A are 1.6% higher than that of stator tooth body when the chopping current threshold is 45A.

### C. INFLUENCE OF HYSTERESIS CURRENT WIDTH ON FLUX DENSITY AND LOSS OF STATOR CORE

The hysteresis current width can affect the loss of stator core. Fig. 8 shows the radial and tangential flux density of the stator core at point A and point B when the hysteresis current width is 0.1A, 0.2A, and 0.3A, respectively. It can be seen from Fig. 8(a) that the radial flux density is relatively high at point A when the hysteresis current width is 0.1A.

Table 7 shows the average values of the radial and tangential flux density at point A and point B under the different hysteresis current widths. When the hysteresis current widths change from 0.1A to 0.2A, the changes of the average value of radial flux density are small at point A and point B. When the hysteresis current width changes from 0.2A to 0.3A, the change of tangential flux density is obvious at point B.

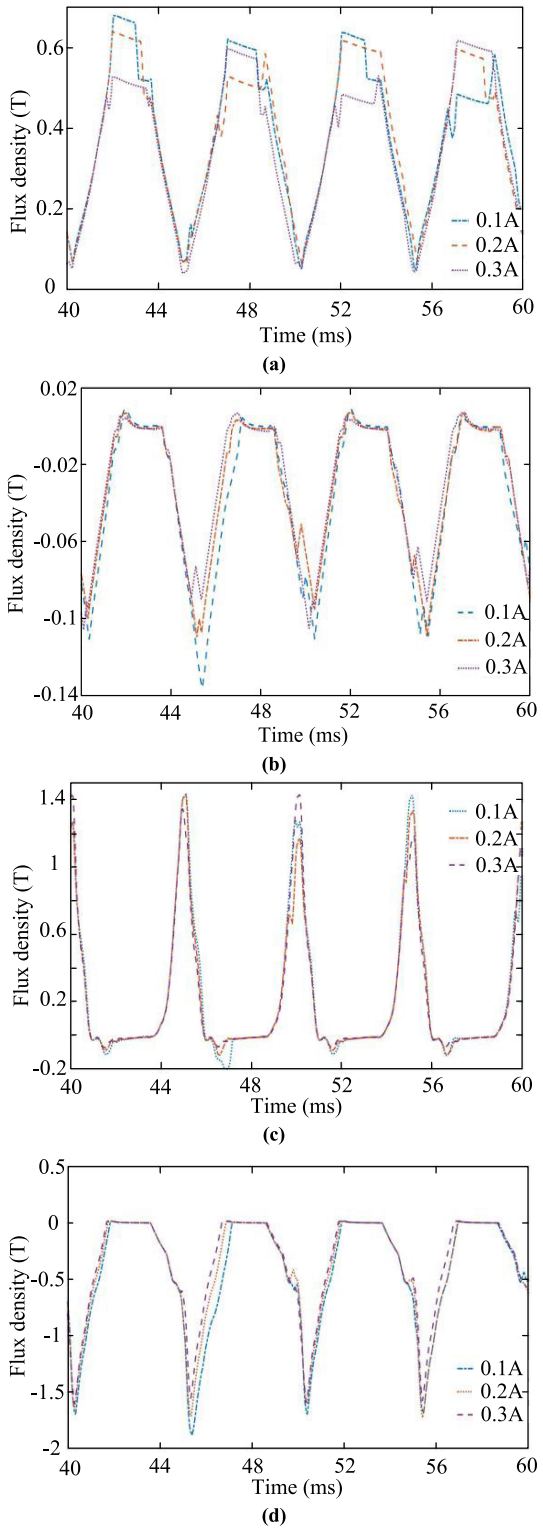


**FIGURE 8.** Radial and tangential flux density of the stator core at point A and point B when the hysteresis current width is 0.1A, 0.2A, and 0.3A, respectively. (a) Radial flux density at point A. (b) Tangential flux density at point A. (c) Radial flux density at point B. (d) Tangential flux density at point B.

Table 8 shows the loss of stator core at different zones at different chopping current thresholds. The change of the

**TABLE 7.** Average values of the radial and tangential flux density at point A and point B under the different hysteresis current widths.

| Flux density (T) | Hysteresis current width (A) | | |
|---|---|---|---|
| | 0.1A | 0.2A | 0.3A |
| Radial flux density at point A | 0.3830 | 0.3843 | 0.3539 |
| Tangential flux density at point A | -0.0366 | -0.0316 | -0.0306 |
| Radial flux density at point B | 0.2211 | 0.2139 | 0.2146 |
| Tangential flux density at point B | -0.4382 | -0.3929 | -0.3528 |

**TABLE 8.** Loss of stator core at different zones under the different hysteresis current widths.

| Hysteresis current widths (A) | Losses of different regions (W) | | | | |
|---|---|---|---|---|---|
| | Stator tooth top | Stator tooth body | Stator inner yoke | Stator outer yoke | Total loss of stator core |
| 0.1A | 6.69 | 42.99 | 23.57 | 13.01 | 86.26 |
| 0.2A | 6.75 | 43.51 | 24.55 | 13.71 | 88.52 |
| 0.3A | 6.80 | 44.32 | 25.02 | 13.98 | 90.12 |

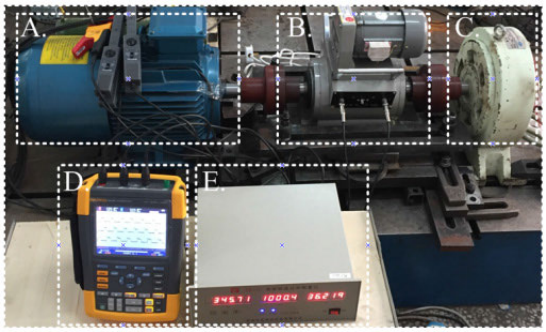


**FIGURE 9.** Prototype and experimental instruments. A. SRM prototype. B. Torque-speed measuring instrument. C. Magnetic powder brake. D. Wave recorder. E. Torque-speed indicator.

hysteresis current width has little effect on the loss of stator core. As the hysteresis current width increases, the total loss of stator core increases. The total loss of stator core when the hysteresis current width is 0.2A are 2.26W higher than that of stator core when the hysteresis current width is 0.1A. The total loss of stator core when the hysteresis current width is 0.3A are 1.6W higher than that of stator core when the hysteresis current width is 0.2A. The loss of the stator inner yoke changes obviously under the different hysteresis current widths.

### D. PROTOTYPE EXPERIMENT AND VERIFICATION

In this paper, a prototype of 5.5kW SRM is manufactured and tested. The prototype and experimental instruments are shown in Fig. 9. In Fig. 9, Letter A-Letter E represent SRM prototype, torque-speed measuring instrument, magnetic powder brake, wave recorder, and torque-speed indicator. The speed, torque, voltage, and current of SRM is measured under the rated operating condition. Fig. 10 shows the rotor and stator of this SRM. Fig. 11 shows the

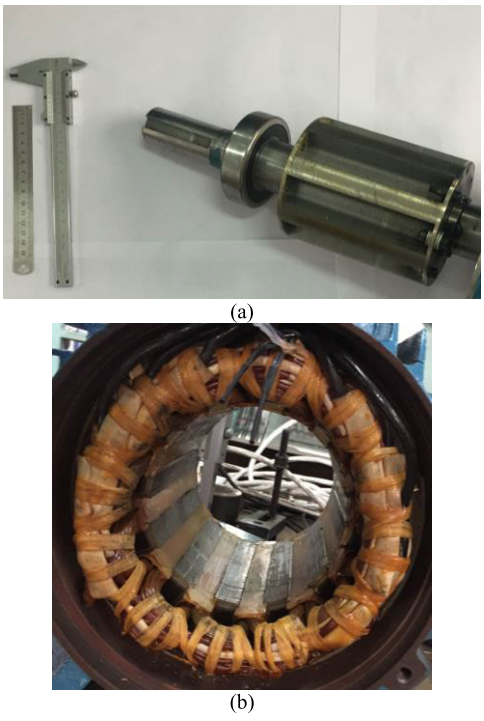

**FIGURE 10.** Rotor and stator of this SRM. (a) Rotor. (b) Stator.

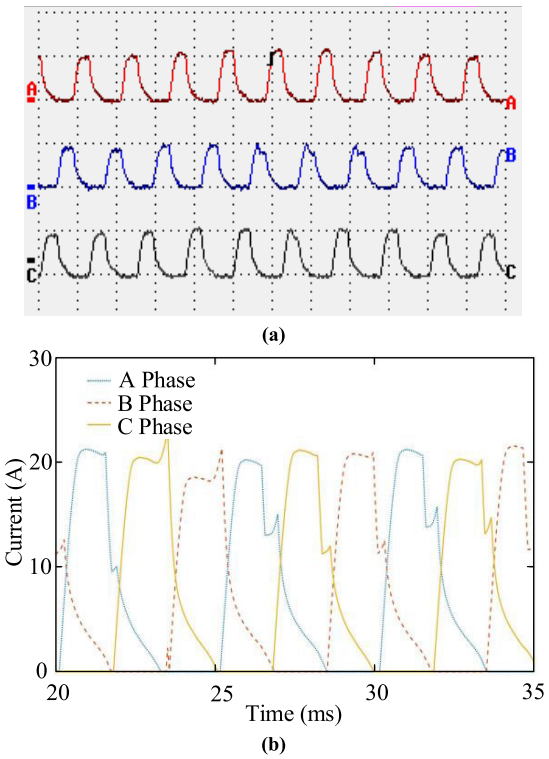


**FIGURE 11.** Measured and calculated current waveform of SRM under the rated operating condition. (a) Measured current waveform of prototype (20A/grid). (b) Calculated current waveform.

measured and calculated current waveform of SRM under the rated operating condition. The measured values are close to calculated results. Fig. 12 show the measured and calculated

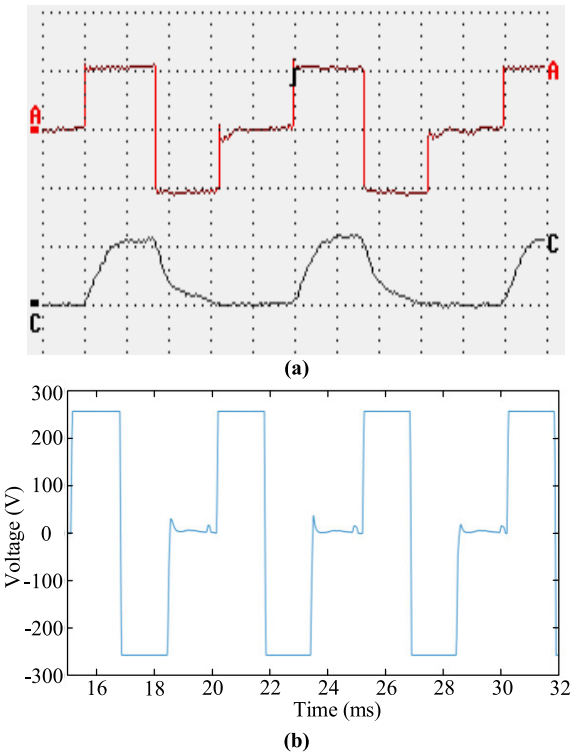


**FIGURE 12.** Measured and calculated voltage waveform of SRM under the rated operating condition. (a) Measured voltage and current waveform of prototype. (Curve A is the voltage waveform, 250V/grid; Curve C is the current waveform, 20A/grid). (b) Calculated voltage waveform.

**TABLE 9.** Measured values and calculated results of SRM.

| | Torque /N·m | Voltage peak value /V | Current peak value /A |
|---|---|---|---|
| Measured values | 34.90 | 513.85 | 21.02 |
| Calculated results | 34.99 | 512.69 | 20.97 |

voltage waveform of SRM under the rated operating condition. The measured values are also close to calculated results. Table 9 gives the measured values and calculated results of SRM under the rated operating condition. The error of the measured values and calculated results is within 3%. It proves that the calculated results and calculation method are accurate and reliable.

The actual measured core loss of the prototype is determined as follows.

$$P_{fe} = P_1 - P_2 - P_{cu} - P_{fv} - P_s \tag{3}$$

According to the measured input voltage, input current, measured output speed, measured output torque, copper loss formula, mechanical loss formula, and stray loss formula, $P_1$, $P_2$, $P_{cu}$, $P_{fv}$, and $P_s$ are obtained. $P_1$ is 6358.9W, $P_2$ is 5431.4W, $P_{cu}$ is 593.6W, $P_{fv}$ is 126.3W, and $P_s$ is 55.65W. The actual measured core loss of the prototype is 151.95W. The calculated core loss is 138.9W. The calculated results conform with the experimental values, which verifies the

reliability of the calculation method and the accuracy of the calculation results.

## IV. CONCLUSION

In this paper, the novel transient electromagnetic field-control circuit coupled calculation method of SRM is proposed. The influence of different PWM switching angles, chopping current thresholds, and hysteresis current widths on the flux density and loss of stator core in the switched reluctance motor is researched in detail. The main conclusions are as follows.

1) The average value of the tangential flux density increases with the decrease of the PWM switching angle at point A. The total loss of stator core is 88.52W, 81.73W, and 77.11W when the PWM switching angle is 16°, 15°, and 14° under the rated operating condition. The losses of stator tooth top, stator tooth body, stator inner yoke, and stator outer yoke when PWM switching angle is 15° are 6.4%, 8%, 6.4%, and 9.6% lower than those of stator tooth top, stator tooth body, stator inner yoke, and stator outer yoke when PWM switching angle is 16°. The total loss of stator core when PWM switching angle is 14° are 5.7% lower than that of stator core when PWM switching angle is 15°.

2) Radial flux density and tangential flux density are the largest at point A when the chopping current threshold is 45A. As the chopping current threshold decreases, the total loss of stator core increases. The loss of stator tooth body when the chopping current threshold is 40A are 1.6% higher than that of stator tooth body when the chopping current threshold is 45A.

3) When the hysteresis current width changes from 0.2A to 0.3A, the change of tangential flux density is obvious at point B. The total loss of stator core when the hysteresis current width is 0.2A are 2.26W higher than that of stator core when the hysteresis current width is 0.1A. The total loss of stator core when the hysteresis current width is 0.3A are 1.6W higher than that of stator core when the hysteresis current width is 0.2A. The loss of the stator inner yoke changes obviously under the different hysteresis current widths. The prototype of 5.5kW SRM is manufactured and tested. The reliability of the calculation method and accuracy of the calculation results are verified by experiment values. The calculated results conform with the measured values.

## REFERENCES

[1] J. F. Pan, F. J. Meng, and N. C. Cheung, "Core loss analysis for the planar switched reluctance motor," *IEEE Trans. Magn.*, vol. 50, no. 2, pp. 813–816, Feb. 2014.

[2] A. A. Memon, S. S. H. Bukhari, and J.-S. Ro, "Experimental determination of equivalent iron loss resistance for prediction of iron losses in a switched reluctance machine," *IEEE Trans. Magn.*, vol. 58, no. 2, pp. 1–4, Feb. 2022.

[3] L. Bernard and L. Daniel, "Effect of stress on magnetic hysteresis losses in a switched reluctance motor: Application to stator and rotor shrink fitting," *IEEE Trans. Magn.*, vol. 51, no. 9, pp. 1–13, Sep. 2015.

[4] V. Rallabandi, J. Wu, P. Zhou, D. G. Dorrell, and D. M. Ionel, "Optimal design of a switched reluctance motor with magnetically disconnected rotor modules using a design of experiments differential evolution FEA-based method," *IEEE Trans. Magn.*, vol. 54, no. 11, pp. 1–5, Nov. 2018.

[5] C. Gan, Y. Chen, X. Cui, J. Sun, R. Qu, and J. Si, "Comprehensive investigation of loss calculation and sequential iterative fluid-solid coupling schemes for high-speed switched reluctance motors," *IEEE Trans. Energy Convers.*, vol. 36, no. 2, pp. 671–681, Jun. 2021.

[6] R. Martin, J. D. Widmer, B. C. Mecrow, M. Kimiabeigi, A. Mebarki, and N. L. Brown, "Electromagnetic considerations for a six-phase switched reluctance motor driven by a three-phase inverter," *IEEE Trans. Ind. Appl.*, vol. 52, no. 5, pp. 3783–3791, Sep./Oct. 2016.

[7] W. Ding, Y. Hu, T. Wang, and S. Yang, "Comprehensive research of modular E-core stator hybrid-flux switched reluctance motors with segmented and nonsegmented rotors," *IEEE Trans. Energy Convers.*, vol. 32, no. 1, pp. 382–393, Mar. 2017.

[8] E. F. Farahani, M. A. J. Kondelaji, and M. Mirsalim, "An innovative hybrid-excited multi-tooth switched reluctance motor for torque enhancement," *IEEE Trans. Ind. Electron.*, vol. 68, no. 2, pp. 982–992, Feb. 2021.

[9] J. Ye, B. Bilgin, and A. Emadi, "Elimination of mutual flux effect on rotor position estimation of switched reluctance motor drives considering magnetic saturation," *IEEE Trans. Power Electron.*, vol. 30, no. 2, pp. 532–536, Feb. 2015.

[10] H. Chen, W. Yan, and K. Wang, "Iron loss analysis of double-sided linear switched reluctance launcher," *IEEE Trans. Plasma Sci.*, vol. 47, no. 5, pp. 2323–2330, May 2019.

[11] G. Davarpanah and J. Faiz, "Nonlinear modeling of a C-core connected two-phase switched reluctance motor," *IEEE Trans. Energy Convers.*, vol. 36, no. 4, pp. 2761–2769, Dec. 2021.

[12] E. Bostanci, M. Moallem, A. Parsapour, and B. Fahimi, "Opportunities and challenges of switched reluctance motor drives for electric propulsion: A comparative study," *IEEE Trans. Transport. Electrific.*, vol. 3, no. 1, pp. 58–75, Mar. 2017.

[13] W. U. N. Fernando and M. Barnes, "Electromagnetic energy conversion efficiency enhancement of switched reluctance motors with zero-voltage loop current commutation," *IEEE Trans. Energy Convers.*, vol. 28, no. 3, pp. 482–492, Sep. 2013.

[14] G. Davarpanah and J. Faiz, "A novel structure of switched reluctance machine with higher mean torque and lower torque ripple," *IEEE Trans. Energy Convers.*, vol. 35, no. 4, pp. 1859–1867, Dec. 2020.

[15] L. Ge, B. Burkhart, and R. W. D. Doncker, "Fast iron loss and thermal prediction method for power density and efficiency improvement in switched reluctance machines," *IEEE Trans. Ind. Electron.*, vol. 67, no. 6, pp. 4463–4473, Jun. 2020.

[16] B. Bilgin, B. Howey, A. D. Callegaro, J. Liang, M. Kordic, J. Taylor, and A. Emadi, "Making the case for switched reluctance motors for propulsion applications," *IEEE Trans. Veh. Technol.*, vol. 69, no. 7, pp. 7172–7186, Jul. 2020.

[17] S. Li, K. W. E. Cheng, N. Cheung, and Y. Zou, "Design and control of a decoupled rotary-linear switched reluctance motor," *IEEE Trans. Energy Convers.*, vol. 33, no. 3, pp. 1363–1371, Sep. 2018.

[18] K. Kiyota, T. Kakishima, A. Chiba, and M. A. Rahman, "Cylindrical rotor design for acoustic noise and windage loss reduction in switched reluctance motor for HEV applications," *IEEE Trans. Ind. Appl.*, vol. 52, no. 1, pp. 154–162, Jan./Feb. 2016.

[19] B. Howey, B. Bilgin, and A. Emadi, "Design of a mutually coupled external-rotor direct drive E-bike switched reluctance motor," *IET Elect. Syst. Transp.*, vol. 10, no. 1, pp. 89–95, Mar. 2020.

[20] H. Ro, D.-H. Kim, H.-G. Jeong, and K.-B. Lee, "Tolerant control for power transistor faults in switched reluctance motor drives," *IEEE Trans. Ind. Appl.*, vol. 51, no. 4, pp. 3187–3197, Jul./Aug. 2015.

[21] M. Asgar, E. Afjei, and H. Torkaman, "A new strategy for design and analysis of a double-stator switched reluctance motor: Electromagnetics, FEM, and experiment," *IEEE Trans. Magn.*, vol. 51, no. 12, pp. 1–8, Dec. 2015.

[22] G. Davarpanah, S. Mohammadi, and J. L. Kirtley, "A novel 8/10 two-phase switched reluctance motor with enhanced performance: Analysis and experimental study," *IEEE Trans. Ind. Appl.*, vol. 55, no. 4, pp. 3402–3410, Jul./Aug. 2019.

[23] E. Gouda and M. Salah H, "A proposed design, implementation and control of doubly fed switched reluctance motor," *CES Trans. Electr. Mach. Syst.*, vol. 3, no. 1, pp. 101–106, Mar. 2019.

[24] A. Stuikys and J. Sykulski, "Rapid multi-objective design optimisation of switched reluctance motors exploiting magnetic flux tubes," *IET Sci., Meas., Technol.*, vol. 12, no. 2, pp. 223–229, Mar. 2018.

**HAN JICHAO** was born in Harbin, China, in 1986. He received the B.S., M.S., and Ph.D. degrees in electrical machinery and appliances from the Harbin University of Science and Technology, Harbin, in 2010, 2013, and 2015, respectively. He is currently a Professor with the Harbin University of Science and Technology. He is the author or coauthor of more than 20 refereed technical articles in IEEE TRANSACTIONS and IET proceedings. He holds more than 20 invention patents. His research interests include research on ventilation cooling, electromagnetics, fluids, and thermal analysis on large electric machine. He was a recipient of the National Scholarship for Doctoral Candidate, in 2012 and 2013.

**WANG JIAOYU** was born in Mudanjiang, China, in 1993. He received the B.S. degree in electrical engineering and automation from the Harbin University of Science and Technology, Harbin, China, in 2016, where he is currently pursuing the M.S. degree in electrical machinery and appliances. His research interests include research on electromagnetics and control on electric machine.

**GE BAOJUN** was born in 1960. He received the B.S. and M.S. degrees in electrical machinery and appliances from the Harbin University of Science and Technology, Harbin, China, in 1982 and 1985, respectively, and the Ph.D. degree in electrical machine and appliances from the Harbin Institute of Technology, Harbin, in 1999. He is currently a Professor with the Harbin University of Science and Technology. He is also the Head of the National High Quality Courses of Electrical Machinery. He is the author or coauthor of more than 100 refereed technical articles and four books. His research interests include new technology of large generator, electromechanical energy conversion, and coordinate theory of generators and power grids.

**QI HAIMING** was born in Qiqihar, China, in 1997. He received the B.S. degree in electrical engineering and automation from the Harbin University of Science and Technology, Harbin, China, in 2021, where he is currently pursuing the M.S. degree in electrical machinery and appliances. His research interests include research on electromagnetics and thermal analysis on electric machine.

**BIAN XIZHAO** was born in Harbin, China, in 1998. He received the B.S. degree in electrical engineering and automation from the Harbin University of Science and Technology, Harbin, in 2020, where he is currently pursuing the M.S. degree in electrical machinery and appliances. His research interests include research on electromagnetics and thermal analysis on electric machine.